

Imaging of MBG starbursts – II. The nature of the sample

Roger Coziol, Clarissa S. Barth[★] and Serge Demers

Département de Physique, Observatoire du Mont Mégantic, Université de Montréal, Montréal, Québec H3C 3J7, Canada

Accepted 1995 May 12. Received 1995 April 25; in original form 1994 May 3

ABSTRACT

In this paper, broad-band imaging in *BVRI* is used in parallel with information from long-slit spectroscopy and *IRAS* data to study star formation processes in a sample of 15 MBG (Montreal blue galaxy) starbursts, in order to understand their nature more clearly. Most of these galaxies are early-type spirals with disturbed morphologies. The burst of star formation is concentrated in the nucleus, extending to a mean distance of 1.6 kpc from the centre. In the most active cases, ionized gas could be detected up to a substantial fraction of the radius of the optical surface of the galaxy. We have found evidence suggesting that the enhancement of star formation in our galaxies is correlated to a higher concentration of gas in the nucleus. No mechanism was clearly identified to explain the accretion of gas in this region. Even though we see MBGs at different levels of activity and with different morphologies, they present similar characteristics in terms of star formation processes.

The peculiar morphologies, the infrared characteristics and the net excess of gas in the MBGs compared with galaxies of the same morphological type suggest that the bursts are related to some kind of interaction with other galaxies. We found near-constant star formation rates over a period of a few Gyr, which we interpret as an indication of either long duration bursts (time-scale of the order 1 Gyr) or a succession of shorter bursts. The concentration of the bursts into the circumnuclear regions and their importance in terms of masses of stars created suggest that this particular phenomenon could represent an important phase in the evolution of these galaxies.

Key words: galaxies: nuclei – galaxies: starburst – galaxies: star clusters.

1 INTRODUCTION

In a previous paper (Barth, Coziol & Demers 1995, hereafter Paper I), we presented the imaging and complete morphological analysis of a sample of 15 starburst nucleus galaxies (SBNGs) from the MBG survey. This sample was composed mainly of early-type spirals with peculiar morphology. The quantitative analysis of Paper I showed that the active star-forming regions in those galaxies are correlated with large isophotal twists. This phenomenon suggests inhomogeneous mass distribution, internal mass transfer or mass accretion. The perturbed morphologies are also related to higher than normal levels of boxiness and discyness of the isophotes. These characteristics, together with the high frequency of dust and the large dispersion of the colours, are usually taken as signs of interacting galaxies. However, in many cases, these

interactions may have taken place a long time ago, because we do not see ongoing merger events, and many galaxies of our sample are isolated.

In this paper, we re-examine the morphology of our sample in parallel with spectroscopic and infrared data, in order to determine the burst characteristics of our sample more accurately and to readdress the question of the nature of these galaxies.

2 OBSERVATIONS

Details on the imaging observations can be found in Paper I, together with a presentation of the results and a quantitative analysis of the morphologies. In parallel with the imaging, the medium-dispersion spectra obtained for the initial spectral classification were used to determine the location and extension of the bursts in the galaxies of our sample. The details on observation and reduction of the spectra can be

[★] Brazilian CNPq fellow; E-mail: clarissa@if.ufrgs.br

found in Coziol et al. (1993, hereafter C93; 1994, hereafter C94). We note that the slit was always oriented E–W, and centred on the most luminous part of the galaxies (usually the nucleus). The aperture of the slit corresponds to 200×2 arcsec² on the sky. For our analysis, we make use of the *IRAS* fluxes taken from the Faint Source Catalogue (Moshir et al. 1989). For all the following calculations, we have used $H_0 = 75 \text{ km s}^{-1} \text{ Mpc}^{-1}$.

2.1 Morphology characteristics of selected MBGs

The different characteristics of each galaxy of the three morphological classes (as defined in Paper I), are presented in Table 1. In column 2, we give the Hubble type of the galaxies, as determined from an inspection of our images. In principle, there is no relation between our classes and the Hubble classification, with the exception that all the late-type spirals will be classified as a spiral. Only eight of our 15 candidates had a Hubble type determined in the literature. For these cases, our determination of the morphology is usually consistent with the classification found, with the exception of the presence of bars, which we detected in three galaxies. The galaxy MBG 03353–2439 was classified in RC3 as a ‘cd’ galaxy, while we classified it as a ‘c’ galaxy, based on the presence of arms. Note that this late-type classification in RC3 does not seem to agree with its $B-V$ colour. In fact, all the late-type spirals in our sample possess $B-V$ colours redder than in normal galaxies of similar morphological types (see Paper I). This may have something to do with the unusual envelope observed in those spirals.

The distances in column 3 and the scalelength in column 4 are determined using the heliocentric velocity (V_h) from C93

and C94, corrected for the motion of the Sun according to $V_0 = V_h + 250 \sin(l) \cos(b)$, where l and b are the galactic longitude and latitude of the objects. The uncertainty on the distance was evaluated as 15 per cent in C93 and C94. The B luminosities, in column 5, are calculated taking into account the extinction inside our galaxy as determined by Burstein & Heiles (1978). With uncertainties of 15 per cent on the distance and 0.1 in the B magnitude, the value $\log(L)$ is known to ± 0.1 . Determination of the stellar masses of our objects (column 6) was carried out using the model estimates of mass-to-light ratio (M_*/L_B) by Larson & Tinsley (1978) for galaxies of different Hubble type. As in the case of the luminosity, the value $\log(M_*)$ is known to ± 0.1 .

Fits of the radial profile of the galaxies with a bulge and an exponential disc were generally unsuccessful (see Paper I). In many cases, model decomposition of the bulges gives high unrealistic characteristic radius (r_c). This ‘false bulge effect’ has been observed in other galaxies by Prieto et al. (1992), and it is probably intrinsic to galaxies with intense star-forming regions. The other difficulty we encountered during model decomposition is related to a proper inclusion of bar profiles. Therefore, in order to compare the light distribution in the galaxies of our sample, we use instead two different spatial parameters. In column 7, we give the ‘maximum radius’ (R_V), determined by the surface brightness curve in the V filter. This radius is defined as the radius of the isophote that has a median flux fluctuation equal to 1σ of the sky. In column 8, we also give the half-width at half-maximum (HWHM) of the galactic luminosity profile $R_{1/2}$. No correction was made to take account of the seeing. The uncertainties on these values are of the order of 15 per cent.

Table 1. Basic parameters of selected MBGs.

MBG	Hubble type	D Mpc	scale pc/arcsec	$\log(L_B)$ L_\odot	$\log(M_{Total})$ M_\odot	R_V kpc	$R_{1/2}$ kpc
AMORPHOUS							
21481-1330	E	151	732	9.69	10.76	6.4	1.8
22106-2410	S0	66	321	9.02	10.09	4.0	0.79
22537-1650	Sab	43	211	9.44	10.24	5.8	0.83
02072-1022	S0 pec	53	255	9.75	10.64	8.7	0.92
PECULIAR							
21513-1623	S0	151	732	9.94	11.02	9.7	1.85
22012-1550	S0(r)	173	841	10.21	11.11	18.6	2.39
23369-2241	SBa pec	110	532	10.03	10.92	10.2	1.4
23382-2047	SB0 pec	126	611	10.02	10.91	14.2	2.15
00461-1259	(R)SB0 pec	70	341	9.80	10.70	8.0	1.44
01166-1719	Sb pec	80	390	10.02	10.82	10.9	1.65
SPIRAL							
21567-1645	SB(r)ab	69	334	9.86	10.66	10.7	0.60
00317-2142	(R')SB(r)bc	110	535	10.36	10.92	16.8	1.11
02141-1134	Sc pec	54	261	9.83	10.38	11.5	0.44
03353-2439	SB(s)c	12	58	9.44	9.69	5.1	0.49
03468-2217	SBa	56	269	9.64	10.54	6.2	0.82

Table 2. Spectroscopic characteristics of selected MBGs.

MBG	$\log(L_{H\alpha})$	<i>SFR</i>	$R_{H\alpha}$		$M_{H\alpha}$	OB stars		$\log(M_{burst})$
	L_{\odot}	$M_{\odot} \text{ yr}^{-1}$	50% <i>kpc</i>	10% <i>kpc</i>	$\times 10^5 M_{\odot}$	number $\times 10^5$	mass $\times 10^5 M_{\odot}$	M_{\odot}
AMORPHOUS								
21481-1330	7.85	1.94	2.45	4.05	37.2	2.3	47.0	9.18
22106-2410	6.50	0.09	0.90	1.45	1.7	1.0	2.1	7.83
22537-1650	6.62	0.11	1.60	2.35	2.3	1.4	2.8	7.95
02072-1022	7.60	3.00	1.25	2.50	60.2	12.7	26.0	8.92
PECULIAR								
21513-1623	7.84	1.86	1.65	3.20	35.6	2.2	45.0	9.15
22012-1550	7.36	0.62	4.15		11.8	7.5	15.0	8.69
23369-2241	7.22	0.45	3.15	4.30	8.8	5.3	11.0	8.54
23382-2047	7.48	0.82	2.10	4.05	16.0	9.9	20.0	8.81
00461-1259	7.29	0.52	1.15	3.20	10.4	6.3	13.0	8.61
01166-1719	7.28	0.52	1.95	3.20	10.3	6.3	13.0	8.61
SPIRAL								
21567-1645	6.56	0.10	0.65		1.9	1.2	2.6	7.93
00317-2142	7.80	1.43	1.45	2.35	28.1	20.5	42.0	9.11
02141-1134	6.94	0.23	0.80	2.85	4.7	2.8	5.7	8.26
03353-2439	5.55	0.01	0.35	1.10	0.2	0.1	0.3	6.95
03468-2217	7.33	0.57	0.60	1.75	11.5	6.8	14.0	8.65

2.2 Spectrophotometric data

In Table 2, we present the spectrophotometric characteristics of our candidates. The $H\alpha$ luminosities were determined using the fluxes published in C93 and C94. The uncertainties on the fluxes are of the order of 20 per cent. Following Hunter & Gallagher (1986), we used these luminosities to estimate the recent star formation rate (SFR) in our galaxies: adopting a Salpeter initial mass function (IMF) with stellar masses between 0.1 and 100 solar masses, the SFR is equal to $7.07 \times 10^{-42} L(H\alpha) M_{\odot} \text{ yr}^{-1}$. The uncertainty on this value is of the order of 20 per cent. The SFRs, given in column 3, are comparable to values determined by other methods. In particular, they are 1.3 times lower than those calculated with the method proposed by Kennicutt (1983), and about 10 times lower than the massive SFRs calculated by Thronson & Telesco (1986) using the infrared luminosities. Note that, because we did not correct the $H\alpha$ fluxes for extinction within the galaxies, these SFRs, and all the other quantities determined similarly, correspond to lower limits.

We use the spatial information of the long-slit spectra to estimate the distribution of the ionized gas in the galaxies (Coziol 1994). In general, the emission is at a maximum in the nucleus. The amorphous galaxies usually have symmetrical distributions. The only exception is MBG 02072 – 1022, which shows emission extending to the west of the nucleus (Paper I). All the peculiar galaxies have disturbed distributions, showing evidence of various kinematical structures. MBG 23369 – 2241 is the only galaxy where the emission does not peak in the nucleus. In fact, there are two peaks, of almost equal intensities and at equal distances on each side of the nucleus, corresponding to a ring circumnuclear region

(Paper I). The spirals also have a disturbed distribution, and in the arms one sees spectroscopic evidence of $H\text{II}$ regions. We give, in columns 4 and 5, the radius of the isophote of the $H\alpha$ emission in the nucleus, measured, respectively, at 50 and 10 per cent of the maximum intensity. No correction was made to take account of the seeing. Uncertainties on these values are of the order of 15 per cent. All the values at 50 per cent are well within the maximum radius of the galaxies and are more extended than the HWHM. For certain galaxies, the intensity at 10 per cent is lost in the continuum, but the more active galaxies have emission that can be detected on a large portion of the surface of the galaxy.

The masses of ionized gas (column 6) were determined following Kim (1989), using the median density found for the MBGs (C94). Knowing these amounts, we can get an idea of the importance of the bursts in terms of the stellar masses involved. First, following Weedman et al. (1981), we determine the number of ionizing photons as $N\alpha = 2.2 \times L(H\alpha) / 3.03 \times 10^{-12} \text{ photon s}^{-1}$ (Pottasch 1965). Then, employing the grid of Panagia (1973), we use these values to determine the present number of OB stars (column 7) and the total mass they represent (column 8). As before, we used for these calculations a Salpeter IMF with stellar masses between 0.1 and 100 M_{\odot} . The total mass of the burst population, between these mass limits, is given in column 9. Uncertainties on the masses are of the order of 20 per cent. The mass values for young stars reported in this paper are generally lower than those estimated by Balzano (1983) for her sample of SBNGs. This difference can be explained both because we did not correct the $H\alpha$ fluxes for internal extinction and because we did not use the same IMF and mass limits. For instance, using a flatter IMF in our calculations increases the

contribution of massive stars, but reduces the total mass of the burst by a factor of 100.

2.3 Infrared data

To complete the view of this sample of MBG starbursts, we give in Table 3 the far-infrared characteristics of our galaxies. All the galaxies are *IRAS* sources, with the exception of MBG 22536–1650. The infrared luminosity (column 4) was determined using only the 60- μm (f_{60}) and 100- μm (f_{100}) fluxes in columns 2 and 3, which are well-determined values for the 14 *IRAS* galaxies of our sample. The luminosity is given by $\log(L_{\text{IR}}) = \log(F_{\text{IR}}) + 2 \log[z(z+1)] + 57.28$, using $F_{\text{IR}} = 1.26 \times 10^{-11} (2.58 f_{60} + f_{100}) \text{ erg cm}^{-2} \text{ s}^{-1}$ (Lonsdale et al. 1985). In column 5, we give the ratios f_{60}/f_{100} , which we will use in our discussion to determine the dominant heating source of the dust in our galaxies. Following Thronson & Telesco (1986), we can estimate the amount of dust using the *IRAS* fluxes at 100 μm . Because this calculation is very sensitive to the dust temperature, we first determine the temperature for each of our galaxies by fitting a blackbody curve on the *IRAS* f_{60} and f_{100} fluxes. The results are given in column 6. The uncertainties of the fit are typically $\pm 1 \text{ K}$. The dust temperatures in our galaxies are comparable to those found for the dust in blue compact dwarfs (BCDs) and irregular galaxies (Thronson & Telesco 1986). Our estimation of the amount of dust is given in column 7. Making the same assumptions as these authors, the dust amount can also be used to get a rough idea of the quantity of neutral gas (H I) present in these galaxies. This estimate is listed in column 8. Based on an uncertainty of $\pm 1 \text{ K}$ for the temperature, the different masses estimated

have a typical uncertainty of 10 per cent. In column 9, we give the neutral gas to stellar mass ratio as M_{HI}/M_{\star} .

3 DISCUSSION

3.1 The morphological characteristics of the MBGs

Our present results reinforce the original findings that the majority of the MBGs are preferentially located in Hubble early-type spiral galaxies (C94). In general, the profiles of the galaxies show a red nucleus and become gradually bluer towards the edge (Paper I). This is exactly the inverse of what is usually observed in BCDs, which are bluer towards the centre (Kunth et al. 1986; Loose & Thuan 1986). In Paper I, we interpreted this phenomenon as the combined effect of extinction by dust and the presence of an older stellar population. In this sense, the host galaxy of the starburst is evolved (also consistent with the near-solar mean metallicity of the MBGs), and thus the present bursts are not primordial.

An examination of Fig. 1(a) shows that our classification of the morphologies is not altered by any bias due to a distance effect. We find galaxies of the three classes at all distances. This leads us to believe that the morphological particularities observed for each class are probably real. In particular, the amorphous class cannot be explained by a lack of resolution, and thus probably reflects a physical property of the galaxies. As we can see in Figs 1(b) and (c), with the exception of MBG 22106–2410, the luminosities and masses of the MBGs of each class are comparable. The least massive galaxies are the amorphous galaxy MBG 22106–2410 (which is also the least luminous) and the spiral MBG 03353–2439. As compared with the other

Table 3. Far-infrared characteristics of selected MBGs.

MBG	f_{60} J_y	f_{100} J_y	$\log(L_{\text{IR}})$ L_{\odot}	f_{60}/f_{100}	T_{dust} K	M_{dust} $\times 10^6 M_{\odot}$	M_{HI} $\times 10^{10} M_{\odot}$	M_{HI}/M_{\star} %
AMORPHOUS								
21481-1330	0.544	1.24	10.41	0.44	35	8.5	1.1	19
22106-2410	0.375	1.18	9.58	0.32	31	2.7	0.3	24
22537-1650								
02072-1022	9.23	20.8	10.70	0.44	35	17.2	2.4	55
PECULIAR								
21513-1623	1.19	2.47	10.74	0.48	36	14.7	1.7	16
22012-1550	0.618	1.33	10.57	0.46	35	12.0	1.3	10
23369-2241	0.590	1.71	10.21	0.35	32	8.8	0.9	11
23382-2047	1.83	3.34	10.72	0.55	38	11.4	1.3	16
00461-1259	1.36	1.97	10.04	0.69	43	2.0	0.3	6
01166-1719	4.06	6.99	10.66	0.58	38	9.8	1.1	17
SPIRAL								
21567-1645	1.15	2.75	10.04	0.42	34	4.5	0.5	11
00317-2142	3.85	8.42	10.97	0.46	35	29.9	4.1	49
02141-1134	5.97	11.8	10.50	0.51	37	8.4	1.0	42
03353-2439	15.9	33.80	9.62	0.47	37	3.7	0.4	82
03468-2217	3.96	5.04	10.28	0.79	45	1.9	0.2	6

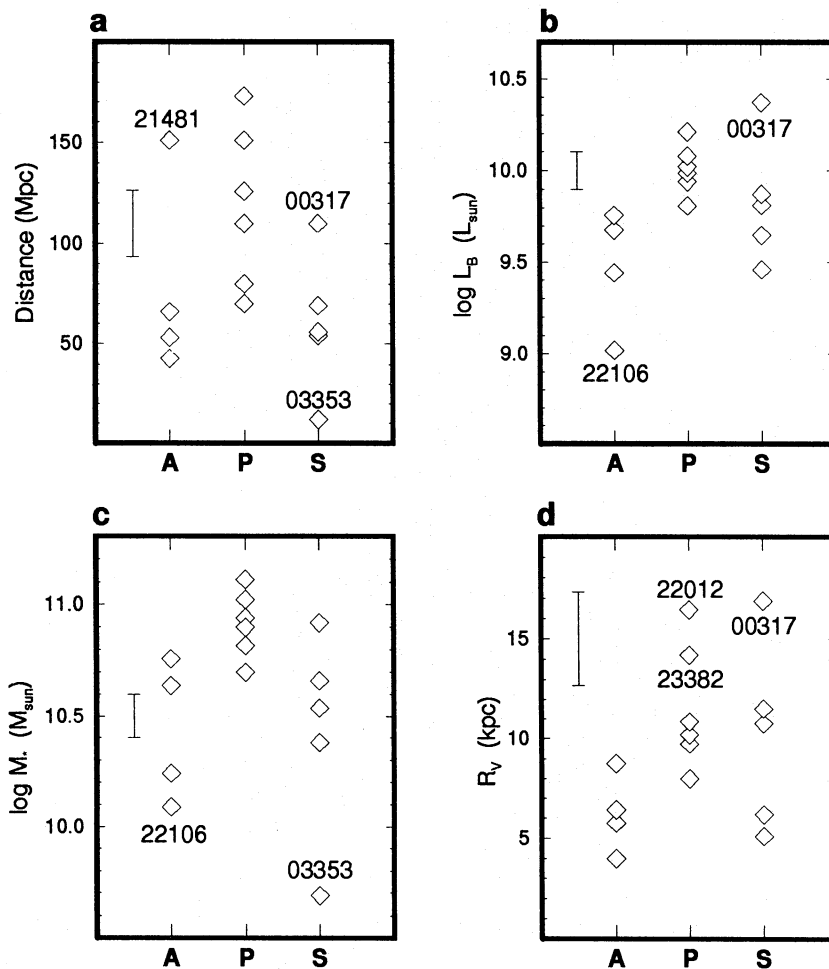


Figure 1. Basic parameters of the galaxies by class: (a) distances; (b) blue luminosities; (c) masses; (d) maximum radii. The error bars represent the typical uncertainties on each value. Note that some of the points have been slightly displaced for clarity.

galaxies of our sample, this particular spiral looks as if it was overluminous for its masses. Fig. 1(d) shows that there are no remarkable differences in the maximum radius of the galaxies of the three classes. The majority of galaxies have a maximum radius smaller than 12 kpc. The three exceptions are the two peculiar galaxies MBG 22012–1550 and 23382–2047, and the spiral galaxy MBG 00317–2142.

Comparison of our results with catalogued galaxies as studied by Roberts & Haynes (1994) suggests that the MBGs of our sample have smaller radii, are less luminous and have lower masses than normal field galaxies of equivalent morphologies. These results are similar to those obtained by Bothun et al. (1989) for the Wasilewski sample of emission-line galaxies. Our galaxies also have higher than average surface brightness, similar to the Wasilewski galaxies (Paper I). The average M_{HI}/M_{\star} ratios for our three classes are 33 per cent for the amorphous, 13 per cent for the peculiar and 38 per cent for the spiral. In general, therefore, the ratios are higher than normal for galaxies of similar morphological types.

3.2 The starburst characteristics of the MBGs

We investigate the location of the bursts, using the ionized gas as a tracer of the star formation regions. Because the

long-slit spectroscopic data used are limited to the central part of the galaxies, the star formation activities that are visible in the disc and the arms of the late-type spiral galaxies of our sample cannot be treated properly in this study. Therefore, our analysis considers only the nucleus and the circumnuclear region. Note, however, that those regions are the most intense star-forming regions in our galaxies.

In Fig. 2(a), we compared the extension of the ionized gas (at 50 per cent intensity) with the maximum radius of the galaxies. In general, the spirals have low ratios, suggesting that the ionized gas is more confined in these objects. Comparable ratios are also found in the amorphous galaxy MBG 02072–1022 and the two peculiar galaxies MBG 00461–1259 and 23382–2047. To check if this confinement also corresponds to a higher concentration of gas, we calculate the ratio of the mass of ionized gas to the total mass of the galaxy. In Fig. 2(b) we see that the amorphous galaxy MBG 02072–1022 shows the highest concentration, with approximately 10 times more ionized gas in its nucleus than any other galaxies. A higher concentration is also suggested for three of the five spiral galaxies and for the two peculiar galaxies MBG 00461–1259 and 23382–2047. On the other hand, the two spiral galaxies MBG 00317–2142 and 03468–2217 possess approximately 10 times less ionized gas in their nucleus than do the other galaxies.

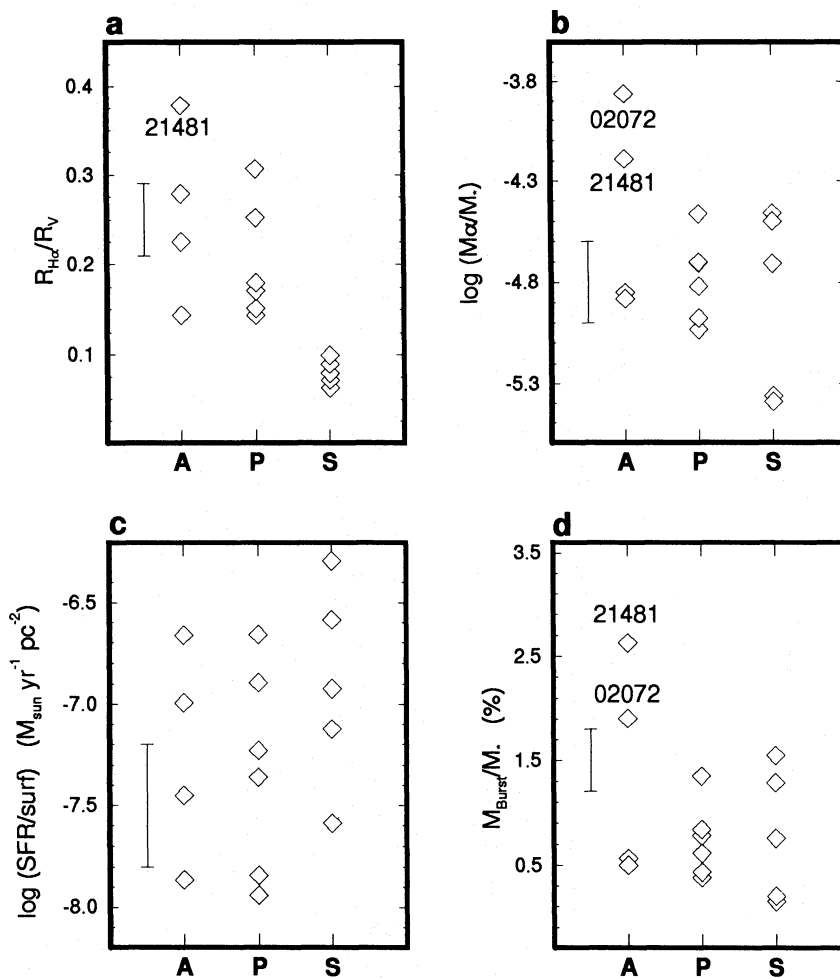


Figure 2. Basic parameters of the galaxies by class: (a) concentration of the ionized gas ($R_{H\alpha}/R_V$); (b) fraction of ionized gas compared with the mass of the galaxy; (c) projected star formation rates per parsec²; (d) mass of the burst population compared with the total mass. The error bars represent the typical uncertainties for each value. Note that some of the points have been slightly displaced for clarity.

It would be interesting to verify whether the concentration of gas observed in some of our galaxies could indicate an enhancement of star formation related to higher gas densities in the nucleus. However, we cannot verify this hypothesis with our data. There are too many difficulties, one of which is that we do not know what is the exact distribution of the gas in the nucleus. However, because the aperture of the slit covers an area comparable to the extent of H α in the nucleus, we are at least assured that there is ionized gas in this area. Therefore, for our objects, we compare instead the density of SFR per parsec². For this calculation, we use the SFR, as determined from the H α emission, and divide it by a projected area, using R_α (50 per cent) as the representative radius of the emission region. We did not correct for the inclination of the galaxies with respect to the plane of the sky because, in the majority of cases, the peculiar morphologies of our candidates simply prevent this kind of correction. As noted before, because we did not correct for internal extinction, those values represent lower limits.

As can be seen in Fig. 2(c), there is no difference in the SFR per parsec² between the galaxies of the different classes. The dispersion is relatively large, the weaker star-forming galaxies having a density of SFR at most, 50 times less than

the stronger star-forming systems in our sample. More interesting, however, is that the spiral galaxies with the lowest ionized gas masses show SFR densities comparable to the other galaxies. The two spiral galaxies with the highest values are, in order of decreasing SFR, MBG 00317–2142 and 03468–2217. With the amorphous galaxy MBG 02072–1022, these two spirals are among the most active star-forming galaxies of our sample. The three galaxies with the more extended emission share the lowest values of SFR densities (the amorphous galaxy MBG 22537–1650 and the two peculiar galaxies MBG 23369–2241 and 22012–1550). From this figure, we conclude that an enhancement of the SFR could be related to the concentration of the gas in the nucleus.

From our data, we cannot identify the cause of the concentration of gas seen in our sample of galaxies. In particular, it is usually believed that a bar could be an efficient mechanism to transport gas towards the centre of a galaxy. In Paper I, we found that all the bar galaxies of our sample show evidence of confinement of the gas in the nucleus. However, we could not distinguish the effect of a bar by using the integrated H α luminosity. Fig. 2(c) suggests the reason: it is because all the galaxies of our sample have

comparable star formation rates in their nuclei. It is possible that part of the dispersion observed in this figure could reflect differences between the detailed mechanisms producing the enhancement of star formation within and around the nucleus of our objects (i.e. differences between the effects of a bar and shocks induced by interaction, and turbulence created by supernovae). Considering the multiple mechanisms possible, it is remarkable that the results in terms of star formation are nevertheless relatively similar.

The strength of the bursts in the galaxies of our sample can be determined by evaluating the mass of the burst stellar population, compared with the luminous mass of the galaxy. The mass of the burst population as a percentage of the total luminous mass of the galaxy is presented in Fig. 2(d). The more active bursts (six out of 15 of the galaxies) represent more than 1 per cent of the actual luminous mass of the host galaxies. The amorphous galaxy MBG 21481–1330 is an example of a global starburst, covering almost its entire surface (see the radius at 10 per cent intensity in Table 3); the burst population represents 2.5 per cent of the stellar mass of the host galaxy.

3.3 The far-infrared emission related to the starbursts

We have already used, in Table 3, the infrared luminosity to determine the dust content of our galaxies and to estimate the amount of neutral gas they contain. To do that, however, we had to assume that most of the far-infrared fluxes come from the dust heated by the massive stars created during the bursts. Supporting this interpretation, we present in Fig. 3 the infrared luminosity as a function of the $H\alpha$ luminosity. As we can see in this figure, most of the galaxies are clustered around the dashed line representing the linear relation $L_{\text{IR}} = 10^3 \times L_{H\alpha}$. The linear coefficient in this relation is 10 times higher than the linear coefficient observed in samples of blue dwarf and irregular galaxies (Thronson & Telesco 1986; Gallagher & Hunter 1987). This is a characteristic of SBNGs (Deutsch & Willner 1986). Considering this higher ratio, it was suggested by different authors that the infrared

excess observed in luminous spirals and irregulars could be due to the heating of dust by an older stellar population. However, if this is the case for SBNGs, we should not see a linear relation between the infrared and the $H\alpha$ luminosities (see Sauvage & Thuan 1992). Therefore, we think that this higher factor observed in general for the SBNGs is more properly explained by a difference in optical depths: SBNGs simply have more dust than BCDs and irregulars. As we can see in Fig. 4(a), the mass of dust implied by the infrared luminosity is comparable in all the galaxies of our sample. There is between 10 and 100 times more dust in these galaxies than in dwarfs and irregulars.

Another way to confirm that in our galaxies the infrared emission is related to the dust associated with the bursts is to check the ratio f_{60}/f_{100} for each of the objects. According to Mazzarella, Bothun & Boroson (1991), this ratio indicates which component of the dust dominates the infrared emission: the warm component of the interstellar radiation

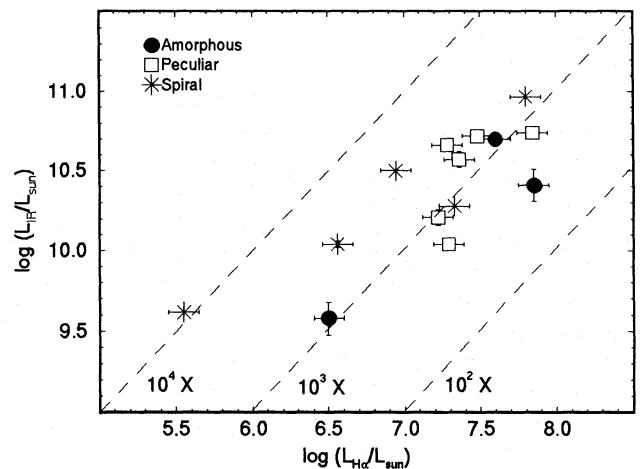


Figure 3. Relation between infrared and $H\alpha$ luminosities. The dashed lines represent the linear relation $L_{\text{IR}} = 10^4, 10^3, 10^2 \times L_{H\alpha}$.

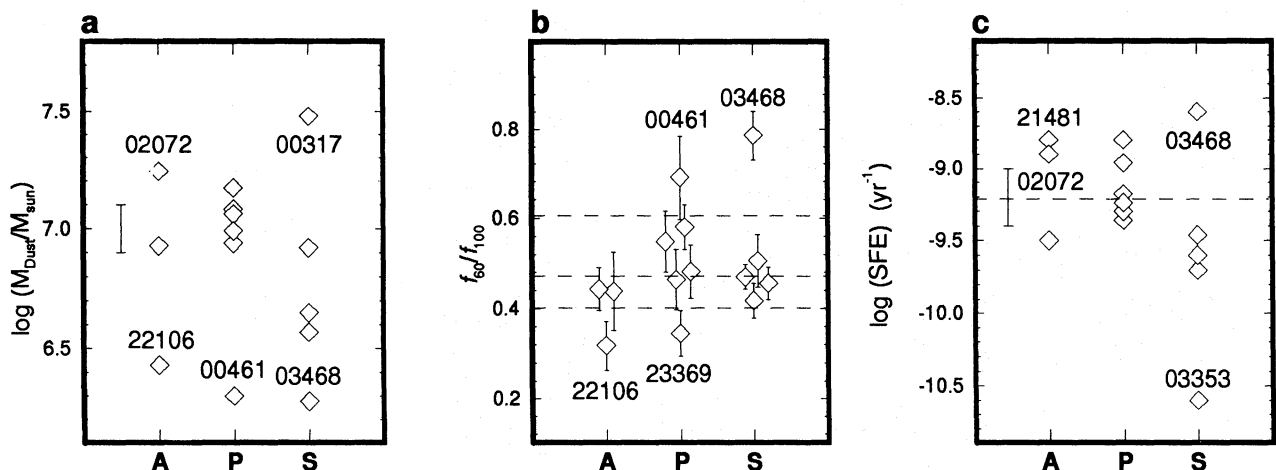


Figure 4. (a) Estimation of dust mass; (b) comparison of the $f_{60\text{-}\mu\text{m}}$ with the $f_{100\text{-}\mu\text{m}}$ fluxes. The dashed lines represent the mean for double nucleus galaxies (0.6), the mean for interacting galaxies (0.47), and the mean for isolated galaxies (0.4) (Mazzarella et al. 1991); (c) star formation efficiencies (SFE). The dashed line represents the characteristic SFE, defined as the SFE corresponding to the relation $L_{\text{IR}} = 10^3 \times L_{H\alpha}$. In each figure the error bar corresponds to the typical uncertainty on the values.

field produced by the newly formed OB stars (more emission at 60 μm) or the cooler cirrus-like component from the dust heated by the diffuse interstellar radiation field (more emission at 100 μm). This ratio is shown in Fig. 4(b). Using the values determined by Mazzarella, Bothun & Boroson (1991), we see that most of our galaxies have ratios higher than or near to the mean found for optically selected interacting galaxies (that is, 0.47). In particular, MBG 00461–1259 has a ratio consistent with its observed double nucleus (higher than 0.60). The two other peculiar galaxies (MBG 23381–2047 and 01166–1719) have the mean value (0.6) and are therefore good candidates for mergers. The galaxy with the highest ratio observed is the spiral MBG 03468–2217. Although it is a relatively high value (0.79), it is none the less lower than the average observed for the ultraluminous infrared galaxies (1.05). This further suggests that none of our objects is heated by an AGN. Two galaxies, MBG 22106–2410 and 23369–2241, have ratios clearly below 0.41, the mean for isolated galaxies. Galaxies with values of this order are the only ones where a greater contribution from an old stellar population is possible. Therefore, there are reasons to believe that, in our galaxies, the dust is generally associated with the young stellar population created by the bursts.

This kind of interpretation is not without problems. For instance, returning to Fig. 3, we can see that not all the galaxies follow the same linear relation. The deviation seems greater for the spiral galaxies. However, as was suggested above, we found no clear evidence of a greater contribution from an old stellar population in those galaxies (see Fig. 4b). In fact, the only two galaxies where a contribution is suspected follow the linear relation $L_{\text{IR}} = 10^3 \times L_{\text{H}\alpha}$. Although we do not have enough information to analyse in depth this peculiar behaviour, we think that the explanation could be related to the particularities observed in the different galaxy classes. In particular, these differences could reflect the different dust distributions (and burst distributions) in the galaxies of each class. For example, in spiral galaxies the bursts are generally concentrated. This suggests that the dust is also more effectively heated and the ionizing efficiency reduced. On the other hand, in galaxies where the bursts are dispersed on very extended regions, the optical depth could be significantly lower and the dust heated less efficiently. This leads to higher $\text{H}\alpha$ fluxes and a lower mean temperature, comparable to cirrus-like components. Obviously, this question will need further investigations.

3.4 The star formation efficiencies (SFEs)

The SFE is defined as the star formation rate estimated from $\text{H}\alpha$ divided by the amount of neutral gas (HI) available (Table 3). For the SFR, we used the value determined in Table 2, but roughly scaled by a factor 10. The reason for this correction is the following. By comparing the ratio of the infrared luminosity and the $\text{H}\alpha$ luminosity, we have found a ratio of 1000, or 10 times higher than what is found in disc HII regions and BCDs. As we have shown above, there is, however, reason to believe that both luminosities are related to the present SFR. Furthermore, the MBGs generally possess more dust than the BCDs. Therefore, it seems reasonable to search for an explanation in terms of a dust effect. Indeed, using the model of Gallagher & Hunter (1987;

see their equation 7), we can reproduce the observed ratio between the two luminosities by changing different parameters related to either the nature of the dust or its distribution. The most simple solution is to suppose that some HII regions in the MBGs are heavily obscured by dust. Consequently, the SFR determined by the $\text{H}\alpha$ should be corrected, following this model, by a factor 10. Note that, corrected this way, the SFRs are now compatible with those found using the IR luminosity directly, as suggested by Thronson & Telesco (1986; see our Section 3.2).

In Fig. 4(c), we see that, with the exception of MBG 03353–2439, the galaxies have comparable SFE values. Because we cannot perform in detail the calculation and because of the way we have estimated the amount of neutral gas in our galaxies, the relatively low SFEs observed for our galaxies have to be accepted with caution. Such as they are, however, our results are comparable to those of Thronson & Telesco (1986) for BCDs and irregular galaxies. This suggests a relatively narrow dispersion for the SFE in active star-forming galaxies in general. Our observations extend similar characteristics to those observed in BCDs and irregulars over four orders of luminosities, both in B and in the infrared.

In Fig. 4(c), the dashed line represents the ‘characteristic SFE’, which is the SFE corresponding to the relation $L_{\text{IR}} = 10^3 \times L_{\text{H}\alpha}$ in Fig. 3. The inverse of the SFE gives us an estimate of the length of time each galaxy would continue to form stars at the rates observed. For this sample, the strongest bursts (MBG 21481–1330) could last 6.3×10^8 yr and transform the equivalent of 16 per cent of the stellar mass of the galaxy into stars. For spirals, the star formation could continue up to 4 Gyr and could transform the equivalent of 38 per cent of the galaxy stellar mass into stars. For our galaxies, the ‘characteristic time’ (defined as the inverse of the characteristic SFE) is 2 Gyr. During this time, a typical burst could transform up to 28 per cent of the galaxy stellar mass into stars.

As we have seen, if the MBGs maintain their present SFRs, the amount of new stars created could be very important. Likewise, it would be interesting to know the duration

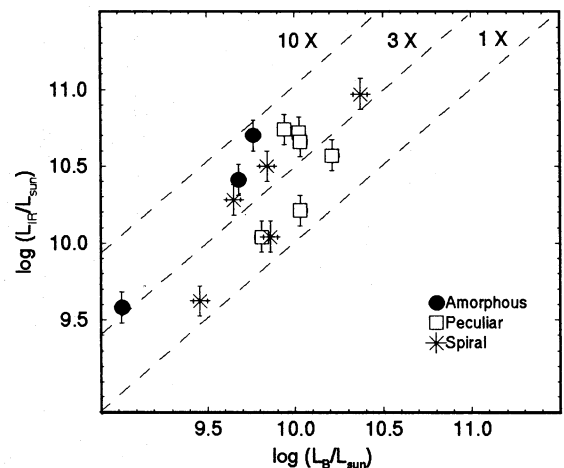


Figure 5. Relation between the infrared and the blue luminosities. A constant star formation rate, over 3 Gyr, corresponds to $L_{\text{IR}} = L_B$. In this diagram, starbursts are defined as galaxies with $L_{\text{IR}} \geq 3 \times L_B$.

of these bursts. We can get an idea of this by comparing, as in Fig. 5, the infrared luminosity of our objects with their luminosity in B . In this paper, we adopt the interpretation made by Thronson & Telesco (1986), that those two luminosities are really measures of galactic star formation rates averaged over significantly different times: the infrared emission comes from regions excited by OB stars, with main-sequence (MS) lifetimes of 10^6 – 10^7 yr, while the blue emission is dominated by main-sequence stars that have MS lifetimes of the order of 1 Gyr and more. Therefore, this figure traces the history of star formation over a few Gyr period.

In Fig. 5, most of our galaxies have a ratio L_{IR}/L_B between 1 and 10. In this figure, galaxies with near-constant SFRs over a time-scale of 3 Gyr should yield $3L_B > L_{\text{IR}} > 1/3L_B$ (Gallagher & Hunter 1987). Consequently, our galaxies have near-constant SFRs over this period. In fact, this is a characteristic of SBNGs in general (Coziol 1994). However, this is also a characteristic of BCDs (Thronson & Telesco 1986) and of irregular galaxies studied by Gallagher & Hunter (1987). Our results extend this observation for BCDs and irregular galaxies in more massive galaxies. Finally, it is interesting to note that near-constant star formation rates are also a characteristic of discs in giant spiral galaxies (Kennicutt 1983). In this case, our results extend this observation to the nucleus of galaxies. It is not clear whether these similarities could signify a similar origin or similar mechanisms behind the process of star formation in all these different galaxies.

3.5 Origin of the bursts in the MBGs

In the case of the MBGs, the problem of a near-constant star formation rate over a period of a few Gyr is, furthermore, complicated not only because the bursts are located in the nucleus of the galaxies, but also by the fact that a majority of these galaxies are early-type spiral galaxies. Indeed, if we consider that the morphology of the host galaxy of our starburst reflects the primordial morphology of the object, we arrive at a contradiction with the classical scenario of galaxy formation of early-type galaxies (Sandage 1986): where does all the extra gas for the burst come from? This leaves us with the only alternative possible, which is the possibility that our galaxies have been gas refuelled during their evolution through some kind of interaction with their environment.

We can test further the hypothesis of an external origin of the gas in our galaxies by comparing the amount of ionized gas present in the MBGs with the amount found for a sample of early-type galaxies compiled by Buson et al. (1993). The galaxies from Buson et al. were selected because they represent early-type galaxies with unusually high activity for galaxies of these morphological types. We reproduced, in Fig. 6, their diagram of the $H\alpha + [\text{N II}]$ luminosities as a function of the absolute B magnitudes, and superposed on it the values of our objects. Dashed lines show the mean relation for a complete sample of E and S0 observed by Phillips et al. (1986). In this figure, we see that most of the early-type galaxies of our sample have a larger fraction of ionized gas. There is 10 times more ionized gas than in the sample of Buson et al., and 200 times more in the MBGs than in normal early-type galaxies. Using the dust as a tracer of atomic and molecular gases, we find a mean $\log(M_{\text{dust}}/L_B)$ ratio of -2.8 ± 0.6 for our sample of early-type galaxies,

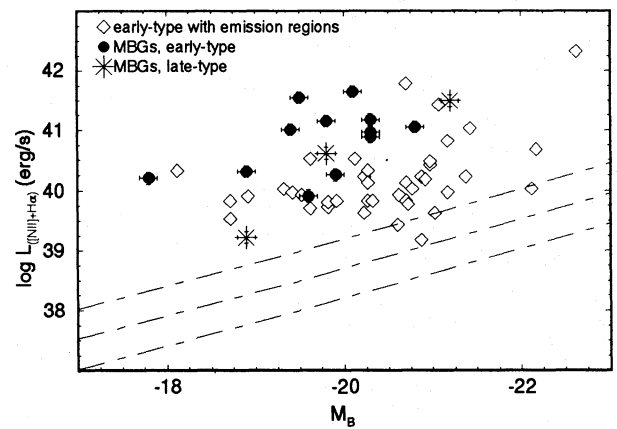


Figure 6. Comparison of the amount of ionized gas in the MBGs of this sample with highly ionized early-type galaxies compiled by Buson et al. (1991). Dashed lines show the mean relation and dispersion for a complete sample of E and S0 galaxies observed by Phillips et al. (1986). The values have been converted to the distance scale used in this paper.

compared with -4.7 ± 0.2 for the sample of Buson et al. and -5.0 ± 0.1 for elliptical and S0 galaxies in general (Bregman, Hogg & Roberts 1992). This represents almost 100 times more dust in our sample than in the sample of Buson et al., and 200 times more than in early-type galaxies in general. Note that the fraction of ionized gas in our objects is still less than 1 per cent of the gaseous mass. Therefore, not only do the MBGs have more ionized gas, but they also possess an overall gas content that is higher than the samples of comparison.

3.6 Significance of the bursts in the MBGs

The huge quantity of gas measured in our galaxies and the fact that most of this gas is concentrated in the nucleus could only mean that this material came from some sort of interaction with other galaxies (see Paper I). Indeed, the alternative would be to suppose a very large amount of neutral gas around our galaxies and very effective mechanisms for draining this gas towards their nuclei. Although this last scenario could work for small galaxies (Taylor, Brinks & Stillman 1993), it seems complicated when applied to more massive objects. In particular, it would be difficult to explain why such a huge quantity of gas did not form a galaxy before. On the other hand, the morphology and environment of our galaxies seem also to suggest that the main interaction event must have taken place several Gyr ago. We probably see interacting galaxies at a later stage of their evolution. They could be the result of the merging of two massive galaxies, or examples of cannibalism of small companion galaxies. Following this interpretation, a near-constant SFR would imply a certain decoupling of the main interaction events from the burst. One possibility is that the bursts are of long duration. Using the model of Charlot & Bruzual (1991), we see that a single burst of star formation gives negative $U-B$ colours (the initial criterion of selection of the MBGs) up to 1.6×10^8 yr, while a 1-Gyr burst gives negative $U-B$ colours up to 1 Gyr. Furthermore, before 1 Gyr, there seems to be no difference between a constant SFR and a 1-Gyr burst.

Therefore, long-duration bursts of the order of 1 Gyr could be possible. As an alternative, one would have to suppose that those galaxies have endured a succession of bursts (Gerola, Seiden & Schulman 1980; Kunth 1989; Krügel & Tutukov 1993).

Considering the characteristic time for the galaxies of our sample found in the previous section, a constant SFR continuing over a 2-Gyr period will transform the equivalent in gas of 28 per cent of the stellar mass of the galaxy into new stars. Now, if we take 1 Gyr as an upper limit for the typical age of a burst in our galaxies and the actual SFR as the mean SFR over this period, we arrive at the conclusion that up to 14 per cent of the actual mass (in stars) of the galaxy could have been created during the present burst. At the end, the completed process, i.e. from the beginning of the burst up to the exhaustion of the gas, could then sum up to 42 per cent of the stellar mass of the galaxy. This is a very high fraction, which suggests that this phenomenon probably represents an important phase in the evolution of those galaxies. Considering that all this star formation is located in the nuclear region, one wonders what the bulge of these galaxies will look like when the burst fades away.

4 CONCLUSION

In this paper, we have studied the characteristics of 15 galaxies from the MBG starbursts in order to understand their nature more clearly and to try to determine the origin of the burst of those galaxies. We have arrived at the conclusion that they are probably examples of different advance stages of evolution of interacting galaxies. In this case, the fact that the SFRs in those galaxies is still high suggests that the burst events are somewhat decoupled from the interaction events. We see two possibilities to explain this phenomenon: either the bursts are of long duration or there was a sequence of bursts. Considering the intensity and duration of the bursts, the creation of new stars in the nuclear region could represent a substantial fraction of the actual stellar mass of the host galaxy, and this phenomenon probably represents an important phase in the evolution of these galaxies.

ACKNOWLEDGMENTS

We acknowledge the support of the staff of the Observatoire du Mont Mégantic. Financial support from the Natural Sciences and Engineering Research Council of Canada and the Québec FCAR is acknowledged. CSB thanks the Brazilian Conselho Nacional de Desenvolvimento Científico e Tecnológico-CNPq for financial support. Thanks are due to the anonymous referee for his comments and suggestions, which have helped to improve this paper. This research has made use of the NASA/IPAC Extragalactic Database (NED), which is operated by the Jet Propulsion Laboratory, Cali-

fornia Institute of Technology, under contract with the National Aeronautics and Space Administration.

REFERENCES

- Balzano V. A., 1983, *ApJ*, 268, 602
 Barth C. S., Coziol R., Demers S., 1995, *MNRAS*, 276, 1224 (Paper I this issue)
 Bothun G. D., Halpern J. P., Lonsdale C. J., Impey C., Schmitz M., 1989, *ApJS*, 70, 271
 Bregman J. N., Hogg D. E., Roberts M. S., 1992, *ApJ*, 387, 484
 Burstein D., Heiles C., 1978, *ApJ*, 225, 40
 Buson L. M. et al., 1993, *A&A*, 280, 409
 Charlot S., Bruzual G. A., 1991, *ApJ*, 367, 126
 Coziol R., 1994, PhD thesis, Université de Montréal
 Coziol R., Demers S., Peña M., Torres-Peimbert S., Fontaine G., Wesemael F., Lamontagne R., 1993, *AJ*, 105, 35 (C93)
 Coziol R., Demers S., Peña M., Barnéoud R., 1994, *AJ*, 108, 405 (C94)
 Deutsch L. K., Willner S. P., 1986, *ApJ*, 306, L11
 Gallagher J. S., Hunter D. A., 1987, in Lonsdale Persson J., ed., *NASA, Washington, Conference Publication 2466, Star Formation in Galaxies*, p. 167
 Gerola H., Seiden P. E., Schulman L. S., 1980, *ApJ*, 242, 517
 Hunter D. A., Gallagher J. S., 1986, *PASP*, 98, 5
 Kennicutt R. C., 1983, *ApJ*, 272, 64
 Kim D.-W., 1989, *ApJ*, 346, 653
 Krügel E., Tutukov A. V., 1993, *A&A*, 275, 416
 Kunth D., 1989, in Beckman J. E., Pagel B. E. J., eds, *Evolutionary Phenomena in Galaxies*. Cambridge Univ. Press, Cambridge, p. 22
 Kunth D., Martin J. M., Maurogordato S., Vigroux L., 1986, in Kunth D., Thuan T. X., Tran Thanh Van J., eds, *First IAP Workshop on Star-Forming Dwarf Galaxies and Related Objects*. Editions Frontières, Paris, p. 89
 Larson R. B., Tinsley B. M., 1978, *ApJ*, 219, 46
 Lonsdale C. J., Helou G., Good J. C., Rice W., 1985, *Cataloged Galaxies and Quasars Observed in the IRAS Survey*. JPL D-1932, Pasadena
 Loose H.-H., Thuan T. X., 1986, in Kunth D., Thuan T. X., Tran Thanh Van J., eds, *First IAP workshop on Star-Forming Dwarf Galaxies and Related Objects*. Editions Frontières, Paris, p. 73
 Mazzarella J. M., Bothun G. D., Boroson T. A., 1991, *AJ*, 101, 2034
 Moshir M. et al., 1989, *IRAS Faint Source Catalog |b| > 10 Degrees, Versions 2.0, Infrared Processing and Analysis Center, Pasadena*
 Panagia N., 1973, *AJ*, 78, 929
 Phillips M. M., Jenkins C. R., Dopita M. A., Sadler E. M., Binette L., 1986, *AJ*, 91, 1062
 Pottasch S. R., 1965, *Vistas Astron.*, 6, 149
 Prieto M., Beckman J. E., Cepa J., Varela A. M., 1992, *A&A*, 257, 85
 Roberts M. S., Haynes M. P., 1994, *ARA&A*, 32, 115
 Sandage A., 1986, *A&A*, 161, 89
 Sauvage M., Thuan T. X., 1992, *ApJ*, 396, L69
 Taylor C. L., Brinks E., Skillman E. D., 1993, *AJ*, 105, 128
 Thronson H. A., Telesco C. M., 1986, *AJ*, 311, 98
 Weedman D. W., Feldman F. R., Balzano V. A., Ramsey L. W., Sramek R. A., Wu C.-C., 1981, *ApJ*, 248, 105